ACS APPLIED MATERIALS & INTERFACES

Letter

www.acsami.org

Facilely Synthesized H-Mordenite Nanosheet Assembly for Carbonylation of Dimethyl Ether

Yahua Liu,[†] Na Zhao,[†] Hui Xian,[‡] Qingpeng Cheng,[†] Yisheng Tan,[§] Noritatsu Tsubaki,[⊥] and Xingang Li*[,†]

[†]Tianjin Key Laboratory of Applied Catalysis Science & Technology, School of Chemical Engineering & Technology, Collaborative Innovation Center of Chemical Science & Engineering (Tianjin), Tianjin University, Tianjin, 300072, P.R. China

[‡]School of Computer Science & Software Engineering, Tianjin Polytechnic University, Tianjin 300387, P.R. China

[§]State Key Laboratory of Coal Conversion, Institute of Coal Chemistry, Chinese Academy of Science, Taiyuan, 030001, P.R. China

[⊥]Department of Applied Chemistry, School of Engineering, University of Toyama, Gofuku 3190, Toyama city, Toyama 930-8555, Japan

Supporting Information

ABSTRACT: Hard coke blockage of micropores of acidic zeolites generally causes serious catalytic deactivation for many chemical processes. Herein, we report a facile method to synthesize H-mordenite nanosheet assemblies without using any template agent. The assemblies exhibit the high catalytic activity for carbonylation of dimethyl ether because of their large quantity of framework Brønsted acids. The specific morphology of the nanosheet unites improves mass diffusion for both reactants and products. Consequently, the coke precursor species can readily migrate from the micropores to the external surface of the assemblies, inducing the improved catalytic stability through inhibiting hard coke formation in frameworks.

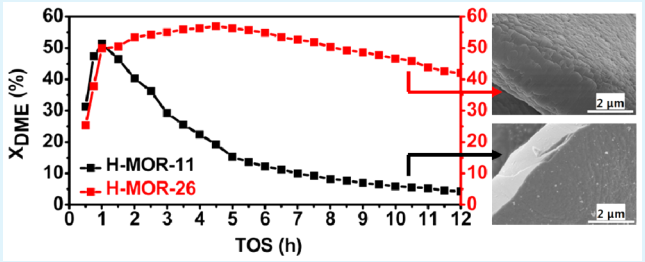

KEYWORDS: *H-mordenite, zeolite, nanosheet, assembly, dimethyl ether, carbonylation, diffusion, coke deposition*

Ethanol is an important clean fuel and chemical material.[1] Its challenging synthesis methodology is strongly in demand.[2] Currently, dimethyl ether (DME) can be easily produced from syngas ($CO+H_2$),[3] which is readily derived from nonedible biomass or cheaper fossil resources such as coal and shale gas, to further selectively synthesize methyl acetate (MA) through carbonylation over H-mordenite (H-MOR) zeolites.[4] Briefly, DME is dissociated to methanol and methoxy species, on which carbon monoxide is inserted to form acetyl species.[5] Thereafter, the acetyl species can react with DME to form MA and regenerate methoxy species.[5] Acids locating in 8-member ring (8-MR) channels of H-MOR were active sites for this process.[6,7] Considering that MA hydrogenation is highly active and selective toward alcohol,[8] we designed a green tandem ethanol synthesis method through DME carbonylation to MA followed by MA hydrogenation to ethanol and methanol, which could be subsequently recycled to DME through dehydration, over the coupled H-MOR and copper-based catalysts.[8−10] It is a promising ethanol synthesis route because of efficient carbon cycle, environmentally friendly reaction conditions and cheap cost.[11]

Unfortunately, the catalytic activity upon DME carbonylation over H-MOR is relatively low.[8,12] Higher reaction temperatures can accelerate the DME carbonylation rates, but bring disadvantages of homologation and oligomerization to form hydrocarbons and hard cokes. This will quickly result in catalytic deactivation, because 8-MR channels in H-MOR are readily blocked by deposited hard cokes therein.[13] Thus, it is urgent to improve the catalytic activity and stability of H-MOR zeolites to realize industrial applications.

Nanosheet morphologies are beneficial to molecular diffusion in microporous zeolites, such as ZSM-5.[14] The reduced crystal sizes can shorten diffusion pathways for coke precursor species migrating out of channels, and then inhibit hard coke formation.[15,16] The crystal size of H-MOR zeolites is generally larger than 10 μm, causing slow mass diffusion. Employing expensive template agents can controllably adjust morphologies and sizes of H-MOR to induce pronouncing performances.[17−19] For example, the H-MOR nanoparticles synthesized with the template of N,N,N,N′,N′,N′-hexaethylpentanediammonium cations showed the higher catalytic performance for DME carbonylation, as compared with conventional big ones.[17] The H-MOR nanosheets synthesized with the template of tetraethylammonium showed the high activity for cracking of cumene.[18] Reducing particle sizes of mordenite membranes using the template of tetraethylammonium bromide enhanced

Received: March 3, 2015
Accepted: April 16, 2015
Published: April 16, 2015

DOI: 10.1021/acsami.5b01905
ACS Appl. Mater. Interfaces 2015, 7, 8398−8403

the H_2/N_2 separation efficiency.[19] However, employing template agents may unfortunately bring disadvantages of high costs, as well as production of aqueous and gaseous pollutions.

Herein, we facilely synthesized H-MOR nanosheet assemblies through a conventional hydrothermal reaction without addition of any template agent. Briefly, the silica gel was slowly dropped into the sodium metaaluminate alkaline solution under continuous stirring. The obtained gel was aged, crystallized, and then calcined to get the H-MOR zeolite samples (see the Supporting Information). The as-synthesized H-MOR zeolite showed the extraordinarily high catalytic activity and stability upon DME carbonylation.

Figure 1 shows the X-ray diffraction (XRD) patterns of the H-MOR zeolites. All of the diffraction peaks belonged to the H-MOR zeolite (JCPDS no. 11−0155), and no other phase was detected. It indicates the successful framework construction of the H-MOR zeolites. The crystallinity of the as-synthesized H-MOR zeolites (Figure 1b−e) decreased with the increasing molar ratio of H_2O/SiO_2 in the raw materials, but was much more complete than that of the commercial nano zeolite H-MOR-C (Figure 1a). It might be due to the usage of the inorganic materials and the presence of the trace amount of NH_4^+ in the raw materials for the as-synthesized zeolites.[20] Additionally, we observed the crystallinity loss after leaching of the H-MOR-11 zeolite, i.e., the H-MOR-11-A, indicating partial destruction of zeolite frameworks.

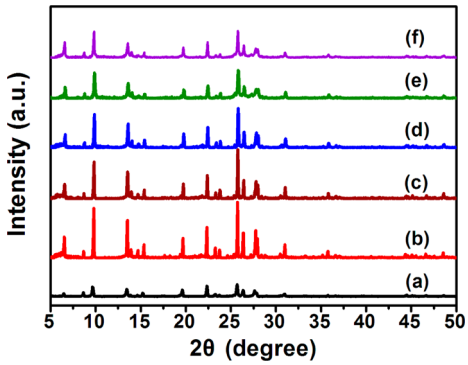

Figure 1. XRD patterns of (a) H-MOR-C, (b) H-MOR-11, (c) H-MOR-20, (d) H-MOR-26, (e) H-MOR-40, and (f) H-MOR-11-A.

Figure S1 in the Supporting Information shows the N_2 physical adsorption/desorption behaviors of the H-MOR zeolites, and these profiles belong to the typical Langmuir-type isotherms. The detailed textual data are listed in Table S1 in the Supporting Information. The as-synthesized H-MOR zeolites possessed the similar BET surface areas, micropore volumes and mesopore volumes. Nevertheless, the S_{ext} value gradually increased from 0.1 (H-MOR-11) to 25.6 $m^2\ g^{-1}$ (H-MOR-40), following the rising molar ratio of H_2O/SiO_2 in the gel systems. After leaching, the H-MOR-11-A got a much larger S_{ext} value of 72.9 $m^2\ g^{-1}$. Considering that the DME carbonylation reaction occurred in the microporous 8-MR channels of the H-MOR zeolites, the larger external surface areas are probably beneficial to mass diffusion for both reactants and products, and may prolong their catalyst life by avoiding coke blockage of micropores of zeolites.

Figure 2 shows the field-emission scanning electron microscopy (FE-SEM) images of the H-MOR zeolites to describe their morphologies. The particle size of the commercial nano H-MOR zeolite was around 100−200 nm (Figure 2a_2). All of the as-synthesized zeolites present the discoidal shapes (Figure 2b_1−e_1). With the rising H_2O/SiO_2 molar ratio in the gel system, the building units evolved from one complete plate with a thickness of around 3 μm to the order nanosheets with a thickness of around 50−100 nm, which assembled to nanosheet bundles (Figure 2b_2−e_2); meanwhile, the mean particle sizes of these nanosheet units decreased (Table S2 in the Supporting Information). Our results indicate that decreasing basicity of the synthesis gel system by diluting

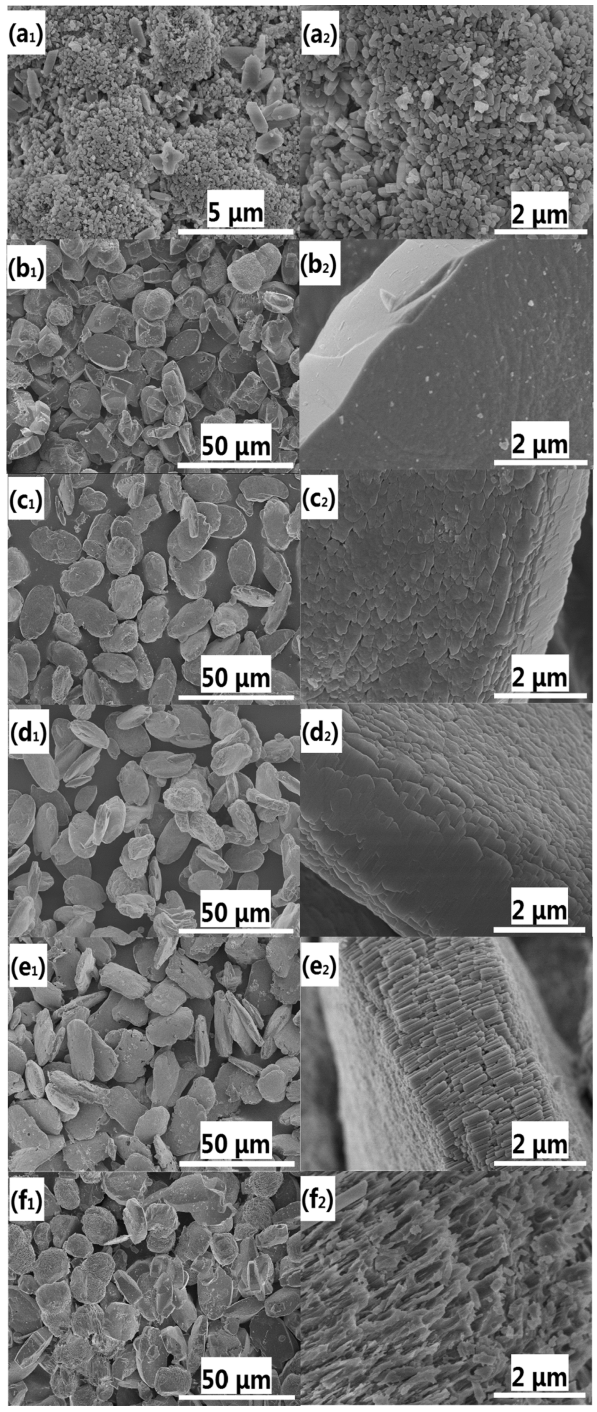

Figure 2. FE-SEM images of (a_1, a_2) H-MOR-C, (b_1, b_2) H-MOR-11, (c_1, c_2) H-MOR-20, (d_1, d_2) H-MOR-26, (e_1, e_2) H-MOR-40, and (f_1, f_2) H-MOR-11-A.

DOI: 10.1021/acsami.5b01905
ACS Appl. Mater. Interfaces 2015, 7, 8398−8403

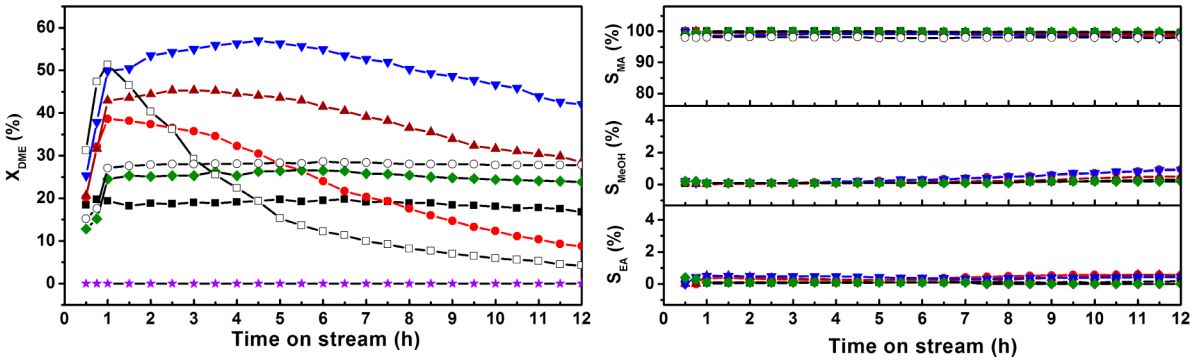

Figure 3. Conversion and product selectivity upon DME carbonylation over (■) H-MOR-C, (●) H-MOR-11, (▲) H-MOR-20, (▼) H-MOR-26, (♦) H-MOR-40, (○) H-MOR-11-A, and (★) Na-MOR-26 at 453 K; and (□) H-MOR-C at 483 K. Reaction conditions: 1.5 MPa, 3 vol % DME/95.5 vol % CO/1.5 vol % N_2, 5280 mL (g h)$^{-1}$.

water favors growth of the H-MOR nano crystals, which then assemble to the nanosheet bundles. Apparently, these H-MOR nanosheet assemblies will expose larger external surface areas (S_{ext}) than those in the shape of the complete plates. The findings are in good agreement with the variation of the S_{ext} values (Table S1 in the Supporting Information). Moreover, as shown in Figure $2f_2$, a lot of pores with a diameter of around 250 nm were generated on the H-MOR-11-A zeolite due to leaching. Accordingly, its S_{ext} value was dramatically enlarged, as compared with the parent H-MOR-11, and became the largest one among the as-synthesized zeolites.

Figure S2 in the Supporting Information shows the FE-SEM images of the H-MOR-26 zeolite synthesized in the different periods to indicate the synthesis mechanism. The amorphous gel was formed with the sizes less than 1 μm (Figure $S2a_2$ in the Supporting Information) after reaction for 12 h, and then it gradually aggregated to the discoidal shape after reaction for 24 h (Figure $S2b_2$ in the Supporting Information). Along the extended reaction period, the amorphous gel disappeared, and the discoidal shape particles grew completely (Figure $S2c_1$,d_1 in the Supporting Information). Meanwhile, these particles were gradually split into nanosheet units, whose thickness evolved from 0.2−1.0 μm to 50−100 nm (Figure $S2c_2$,d_2 in the Supporting Information).

We plotted Arrhenius curves of the H-MOR zeolites for DME carbonylation to MA in Figure S3 in the Supporting Information. They presented the similar activation energy values (59.8−62.1 kJ mol^{-1}), regardless of their different morphologies. These values are quite close to the reported data.[5] It demonstrates that these zeolites follow the same reaction rules, and the catalytic activity is only determined by the number of the active sites, i.e., the effective acidic sites.

Figure 3 shows the catalytic activity of DME carbonylation over the mordenite zeolites. Herein, the Na-MOR-26, the precursor of H-MOR-26 without ion-exchange, was completely catalytically inactive, demonstrating the significant roles of the ion-exchanged H^+, which directly relates to the framework Brønsted acids. Over each H-MOR zeolites, the MA selectivity in products was more than 98% with a trace amount of methanol and ethyl acetate (EA) byproducts. The formation of EA is probably due to the reaction between the methyl species and MA.

For the H-MOR-C zeolite, the DME conversion was constant at about 19% at 453 K. It could further rise to 50% by increasing the reaction temperature to 483 K; nevertheless, this would result in the dramatically catalytic deactivation. As for the as-synthesized H-MOR zeolites, the catalytic activity of DME carbonylation was significantly enhanced at the induction period, as compared with the H-MOR-C zeolite. The DME conversion of the H-MOR-11 sharply dropped from 39% (after 2 h) to 9% (after 12 h); meanwhile, the DME conversions over the H-MOR-26 sample got stable at around 42% after 12 h. The DME conversion of the H-MOR-40 maintained at about 26% in the whole reaction test. Interestingly, the strong acid and alkali solution treated H-MOR-11-A zeolite also exhibited the excellent catalytic stability, and its DME conversion kept constant at around 29%. As compared with the H-MOR-11 zeolite, the H-MOR-11-A zeolite had the larger S_{ext} value (Table S1 in the Supporting Information) and was more catalytically stable (Figure 3). We can draw a conclusion that the external surface area plays the important role to the catalytic stability of the H-MOR zeolites, and the larger S_{ext} value will result in the longer catalyst life. Thus, the commercial H-MOR-C also exhibited the excellent catalytic stability, because of its large S_{ext} value.

Figure S4 in the Supporting Information gives the temperature-programmed desorption of ammonia (NH_3-TPD) profiles of the zeolites to determine their acidic features. In Figure S4a−e in the Supporting Information, all profiles of the H-MOR zeolites exhibit the similar ammonia desorption behaviors. The deconvoluted peak P_1, P_2, and P_3, following the increased desorption temperatures, correlates to the weak, moderate and strong acidic sites on zeolites, respectively. Figure S4g in the Supporting Information clearly shows that no strong acidic site existed on the Na-MOR-26 zeolite, which was catalytically inert upon DME carbonylation (Figure 3). Thus, these strong acidic sites (peak P_3) should belong to the framework Brønsted acid, as it appeared after Na-MOR ion-exchanged to H-MOR, whereas the weak and moderate acids mainly existed on the external surface areas. Table 1 provides the quantitative amount of these acidic sites. The quantity of the strong Brønsted acidic sites directly linked to the catalytic activity after the induction period in Figure 3, i.e., H-MOR-26 > H-MOR-20 > H-MOR-11 > H-MOR-11-A > H-MOR-40 > H-MOR-C. However, the weak and moderate acids did not follow this tendency. It demonstrates that upon DME carbonylation, the catalytic activity was determined by the quantity of the framework Brønsted acidic sites, instead of the weak and moderate acidic sites on the external surface.

Before the NH_3-TPD experiments, the spent H-MOR zeolites were dried at 383 K for 12 h and then calcined in air at 823 K for 3 h. Compared with the corresponding fresh

DOI: 10.1021/acsami.5b01905
ACS Appl. Mater. Interfaces 2015, 7, 8398−8403

Table 1. Quantities of the Acidic Sites Determined by NH_3-TPD in Figure S4 in the Supporting Information

sample	quantity of acidic sites (mmol g^{-1})		
	weak	moderate	strong
fresh H-MOR-C	0.131	0.018	0.470
fresh H-MOR-11	0.152	0.085	0.833
fresh H-MOR-20	0.179	0.128	0.893
fresh H-MOR-26	0.288	0.093	1.004
fresh H-MOR-40	0.156	0.088	0.527
fresh H-MOR-11-A	0.154	0.106	0.623
fresh Na-MOR-26	0.270	0.350	0.000
spent H-MOR-C	0.172	0.048	0.140
spent H-MOR-11	0.240	0.068	0.411
spent H-MOR-26	0.192	0.064	0.545
spent H-MOR-40	0.161	0.062	0.512

zeolites, the quantity of the strong Brønsted acidic sites on the spent ones decreased, while little difference was observed for the weak and moderate acids. It also indicates that the strong Brønsted acids are the active sites during DME carbonylation. The decreased quantity is probably due to the occupation of the remained cokes on them.[21]

To illuminate the framework characteristics of the as-synthesized zeolites, Figure S5 in the Supporting Information shows their solid-state ^{29}Si and ^{27}Al magic-angle spinning nuclear magnetic resonance (MAS NMR) spectra. In Figure S5A in the Supporting Information, the ^{29}Si MAS NMR spectra were deconvoluted to four Gaussian peaks at about −112, −106, −102, and −99 ppm, which could be assigned to Si(0Al), Si(1Al), Si−OH, and Si(2Al) unit, respectively.[22] Among these Si units, the Si(1Al) and Si(2Al) afford the framework Brønsted protons in zeolites. The relative intensity of the Si(1Al) and Si(2Al) peaks of the H-MOR-20 and H-MOR-26 zeolites, especially the H-MOR-26, was more pronounced than others (Figure S5A in the Supporting Information), indicating the existence of more framework Brønsted acidic sites. The lower qualitative ratio of Si and Al atoms in frameworks, i.e., the $(Si/Al)_f$ ratio,[23] would result in the larger amount of framework Brønsted acidic sites. In Figure S5B in the Supporting Information, the ^{27}Al MAS NMR spectra show that more extra-framework Al atoms existed on the H-MOR-40 and H-MOR-11-A zeolites, which coincided with the $(Si/Al)_f$ ratio listed in Table S2 in the Supporting Information. These findings are in good agreement with the quantity of the strong Brønsted acidic sites of the H-MOR zeolites (Table 1).

To identify the coke formation on the H-MOR zeolites, Figure 4 shows their temperature-programmed oxidation (TPO) profiles. The signal of m/e = 44 was recorded to qualitatively determine the generated CO_2, while the signal of m/e = 18 was recorded for the produced H_2O. No CO_2 signal was detected on the TPO profile of the fresh H-MOR-26, and desorption of H_2O at above 850 K was due to dehydration of surface O−H species on zeolite. As for the spent H-MOR zeolites, the CO_2 signal appeared in the temperature range of 450−980 K. Generally, the low-temperature (LT) CO_2 desorption peaks ranging 450−750 K are attributed to combustion of soft cokes, whereas the high-temperature (HT) CO_2 desorption peaks ranging 750−980 K are ascribed to combustion of hard cokes.[17,24] Herein, the soft coke was originated from combustion of the adsorbed reaction intermediates, e.g., surface methyl and acetyl species, so that the LT CO_2 desorption peaks located at the similar

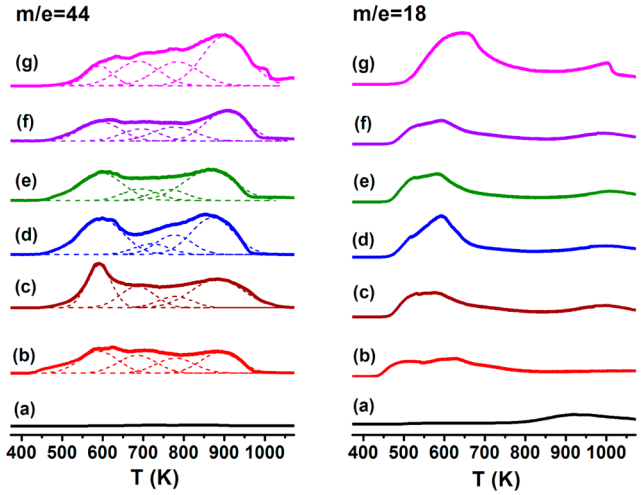

Figure 4. TPO profiles of (a) the fresh H-MOR-26 and the spent H-MOR zeolites: (b) H-MOR-C, (c) H-MOR-11, (d) H-MOR-20, (e) H-MOR-26, (f) H-MOR-40, and (g) H-MOR-11-A.

temperatures for all of the spent H-MOR zeolites, associating with generation of H_2O. Nevertheless, the location of the HT CO_2 desorption peaks obeyed the sequence of H-MOR-40 > H-MOR-11 > H-MOR-26 ≈ H-MOR-20; meanwhile, little H_2O was generated at the temperature range except from dehydration of zeolite. It further confirms that the HT CO_2 peak in Figure 4 for the spent H-MOR zeolites is originated from combustion of the hard coke. Interestingly, as compared with the H-MOR-11 zeolite, the position of the LT peak of the H-MOR-11-A had little change, but its HT peak shifted toward the higher temperatures in Figure 4. This difference must be induced by the enlarged external surface area of the H-MOR-11-A (Table S1 in the Supporting Information). Accordingly, as for the H-MOR-C, the position of the HT peak located at higher temperatures because of its relatively bigger S_{ext} value (Table S1 in the Supporting Information).

Previous studies on H-ZSM-5 and H-BEA zeolites showed that intermediate species generated in framework micropores could partially migrate to external surfaces, and then form polyaromatic molecules, which became heavier with enlarged external surface areas and prolonged reaction periods.[25,26] Additionally, soft cokes formed on strong framework acidic sites of H-ZSM-5 could progressively migrate to weak acidic sites and then form hard cokes.[27] Upon DME carbonylation, the migration of acetyl groups from 8-MR channels to 12-MR channels in H-MOR had been evidenced by NMR.[7] Probably, the intermediate groups such as methoxy and acetyl could further migrate from the strong framework acidic sites to the weaker acidic sites on the external surface, and then act as precursors to generate heavy molecules, i.e., hard cokes. Because of lacking steric constraints for growth of coke molecules, the larger external surface areas will result in deposition of the more hard cokes with heavier molecular weights. This assumption can well-explain our TPO results in Figure 4. The H-MOR-40 and H-MOR-11-A zeolites had the larger external surface areas, as compared with other as-synthesized zeolites (Table S1 in the Supporting Information). Thus, the former spent zeolites had the relatively larger hard coke proportion, and their HT peaks shifted toward the higher temperatures, because of formation of the heavier hard cokes. Thus, the HT peak of the H-MOR-C located at higher temperatures because of its relatively bigger S_{ext} value (Table S1

DOI: 10.1021/acsami.5b01905
ACS Appl. Mater. Interfaces 2015, 7, 8398−8403

in the Supporting Information). As for the H-MOR-11 zeolite, the coke precursor species difficultly migrated to its external surface because of its big crystal size and small S_{ext} value, and thus the hard coke mainly formed inside of frameworks. Accordingly, although the amount of the hard coke was small, it would quickly block the microporous channels of the H-MOR-11, inducing the serious deactivation (Figure 3).

In summary, we successfully synthesized H-mordenite nanosheet assemblies through a hydrothermal reaction. This facile synthesis methodology is free of template agents, and thus avoids disadvantages of high costs and pollution emissions. Upon DME carbonylation, the catalytic activity of the H-MOR-26 nanosheet assemblies is more than twice higher compared with the commercial nano H-MOR zeolite because of the former's larger amount of the framework Brønsted acidic sites. Additionally, the specific morphology of the H-MOR nanosheet assemblies shows the excellent catalytic stability by improving mass diffusion. The coke precursor species can easily migrate from the micropores to the external surface, inhibiting hard coke blockage in zeolite frameworks. Perspectively, the H-mordenite nanosheet assembly can be potentially applied in separation and other chemical processes.

■ ASSOCIATED CONTENT

Supporting Information

Detailed experimental section, Tables S1 and S2, and Figures S1–S5. This material is available free of charge via the Internet at http://pubs.acs.org/.

■ AUTHOR INFORMATION

Corresponding Author

*E-mail: xingang_li@tju.edu.cn.

Notes

The authors declare no competing financial interest.

■ ACKNOWLEDGMENTS

This work was financially supported by the National Natural Science Foundation of China (21476159), the 973 program (2014CB932403), the Program for Introducing Talents of Discipline to Universities of China (B06006), and the Foundation of State Key Laboratory of Coal Conversion (J15-16-902).

■ REFERENCES

(1) Schmidt, L. D.; Dauenhauer, P. J. Hybrid Routes to Biofuels. *Nature* **2007**, *447*, 914–915.

(2) Spivey, J.; Egbebi, A. Heterogeneous Catalytic Synthesis of Ethanol from Biomass-Derived Syngas. *Chem. Soc. Rev.* **2007**, *36*, 1514–1528.

(3) Jeong, J. W.; Ahn, C.; Lee, D. H.; Um, S. H.; Bae, J. W. Effects of Cu-ZnO Content on Reaction Rate for Direct Synthesis of DME from Syngas with Bifunctional Cu-ZnO/γ-Al_2O_3 Catalyst. *Catal. Lett.* **2013**, *143*, 666–672.

(4) Cheung, P.; Bhan, A.; Sunley, G. J.; Iglesia, E. Selective Carbonylation of Dimethyl Ether to Methyl Acetate Catalyzed by Acidic Zeolites. *Angew. Chem., Int. Ed.* **2006**, *45*, 1617–1620.

(5) Cheung, P.; Bhan, A.; Sunley, G. J.; Law, D. J.; Iglesia, E. Site Requirements and Elementary Steps in Dimethyl Ether Carbonylation Catalyzed by Acidic Zeolites. *J. Catal.* **2007**, *245*, 110–123.

(6) Boronat, M.; Martinez-Sanchez, C.; Law, D.; Corma, A. Enzyme-Like Specificity in Zeolite: a Unique Site Position in Mordenite for Selective Carbonylation of Methanol and Dimethyl Ether with CO. *J. Am. Chem. Soc.* **2008**, *130*, 16316–16323.

(7) Li, B. L.; Xu, J.; Han, B.; Wang, X. M.; Qi, G. D.; Zhang, Z. F.; Wang, C.; Deng, F. Insight into Dimethyl Ether Carbonylation Reaction over Mordenite Zeolite from In-Situ Solid-State NMR Spectroscopy. *J. Phys. Chem. C* **2013**, *117*, 5840–5847.

(8) Li, X. G.; San, X. G.; Zhang, Y.; Ichii, T.; Meng, M.; Tan, Y. S.; Tsubaki, N. Direct Synthesis of Ethanol from Dimethyl Ether and Syngas over Combined H-Mordenite and Cu/ZnO Catalysts. *ChemSusChem* **2010**, *3*, 1192–1199.

(9) Yang, G. H.; San, X. G.; Jiang, N.; Tanaka, Y.; Li, X. G.; Jin, Q.; Tao, K.; Meng, F. Z.; Tsubaki, N. A New Method of Ethanol Synthesis from Dimethyl Ether and Syngas in a Sequential Dual Bed Reactor with the Modified Zeolite and Cu/ZnO Catalysts. *Catal. Today* **2011**, *164*, 425–428.

(10) San, X. G.; Zhang, Y.; Shen, W. J.; Tsubaki, N. New Synthesis Method of Ethanol from Dimethyl Ether with a Synergic Effect between the Zeolite Catalyst and Metallic Catalyst. *Energy Fuels* **2009**, *23*, 2843–2844.

(11) Haro, P.; Ollero, P.; Villanueva, A. V.; Gomez-Barez, A. Thermochemical Biorefinery Based on Dimethyl Ether as Intermediate Technoeconomic Assessment. *Appl. Energy* **2013**, *102*, 950–961.

(12) Bhan, A.; Allian, D.; Sunley, G. J.; Law, D. J.; Iglesia, E. Specificity of Site within Eight-Membered Ring Zeolite Channels for Carbonylation of Methyls to Acetyls. *J. Am. Chem. Soc.* **2007**, *129*, 4919–4924.

(13) Liu, J. L.; Xue, H. F.; Huang, X. M.; Wu, P. H.; Huang, S. J.; Liu, S. B.; Shen, W. J. Stability Enhancement of H-Mordenite in Dimethyl Ether Carbonylation to Methyl Acetate by Pre-adsorption of Pyridine. *Chin. J. Catal.* **2010**, *31*, 729–738.

(14) Choi, M.; Na, K.; Kim, J.; Sakamoto, Y.; Terasaki, O.; Ryoo, R. Stable Single-Unit-Cell Nanosheets of Zeolite MFI as Active and Long-Lived Catalysts. *Nature* **2009**, *461*, 246–251.

(15) Tago, T.; Konno, H.; Sakamoto, M.; Nakasaka, Y.; Masuda, T. Selective Synthesis for Light Olefins Acetone over ZSM-5 Zeolite with Nano- and Macro-Crystal Sizes. *Appl. Catal., A* **2011**, *403*, 183–191.

(16) Jang, H. G.; Min, H. K.; Lee, J. K.; Hong, S. B.; Seo, G. SAPO-34 and ZSM-5 Nanocrystals' Size Effects on their Catalysis of Methanol-to-Olefin Reactions. *Appl. Catal., A* **2012**, *437–438*, 120–130.

(17) Xue, H. F.; Huang, X. M.; Ditzel, E.; Zhan, E. S.; Ma, M.; Shen, W. J. Dimethyl Ether Carbonylation to Methyl Acetate over Nanosized Mordenite. *Ind. Eng. Chem. Res.* **2013**, *52*, 11510–11515.

(18) Inagaki, S.; Watanabe, Y.; Nishita, Y.; Kubota, Y. Synthesis of Mordenite Nanocrystals by Using a Hydrophobic Structure-Directing Agent. *Chem. Lett.* **2013**, *42*, 186–188.

(19) Zhang, Y.; Xu, Z.; Chen, Q. Synthesis of Small Crystal Polycrystalline Mordenite Membrane. *J. Membr. Sci.* **2002**, *210*, 361–368.

(20) Lu, B. W.; Oumi, Y.; Itabashi, K.; Sano, T. Effect of Ammonium Salts on Hydrothermal Synthesis of High-Silica Mordenite. *Microporous Mesoporous Mater.* **2005**, *81*, 365–374.

(21) Pour, A. N.; Housaindokht, M. R. Fischer–Tropsch Synthesis on Iron Catalyst Promoted with HZSM-5 Zeolite: Regeneration Studies of Catalyst. *J. Nat. Gas Sci. Eng.* **2013**, *14*, 49–54.

(22) Xue, H. F.; Huang, X. M.; Zhan, E. S.; Ma, M.; Shen, W. J. Selective Dealumination of Mordenite for Enhancing its Stability in Dimethyl Ether Carbonylation. *Catal. Commun.* **2013**, *37*, 75–79.

(23) Zheng, A. M.; Huang, S. J.; Wang, Q.; Zhang, H. L.; Deng, F.; Liu, S. B. Progress in Development and Application of Solid-State NMR for Solid Acid Catalysis. *Chin. J. Catal.* **2013**, *34*, 436–491.

(24) Palumbo, L.; Bonino, F.; Beato, P.; Bjørgen, M.; Zecchina, A.; Bordiga, S. Conversion of Methanol to Hydrocarbons: Spectroscopic Characterization of Carbonaceous Species Formed over H-ZSM-5. *J. Phys. Chem. C* **2008**, *112*, 9710–9716.

(25) Pinard, L.; Hamieh, S.; Canaff, C.; Madeira, F. F.; Gener, I.; Maury, S.; Delpoux, O.; Tayeb, K. B.; Pouilloux, Y.; Vezin, H. Growth Mechanism of Coke on HBEA Zeolite during Ethanol Transformation. *J. Catal.* **2013**, *299*, 284–297.

DOI: 10.1021/acsami.5b01905
ACS Appl. Mater. Interfaces 2015, 7, 8398–8403

(26) Anderson, J. R.; Chang, Y. F.; Western, R. J. Retained and Desorbed Products from Reaction of 1-Hexene over H-ZSM-5 Zeolite: Routes to Coke Precursors. *J. Catal.* **1989**, *118*, 466−482.
(27) Bibby, D. M.; Milestone, N. B.; Patterson, J. E.; Aldridge, L. P. Coke Formation in Zeolite ZSM-5. *J. Catal.* **1986**, *97*, 493−502.

DOI: 10.1021/acsami.5b01905
ACS Appl. Mater. Interfaces 2015, 7, 8398−8403